Article:
Whitley, DM and Adolf, DB (2010) Barrier properties of polyethylene terephthalate, atactic polypropylene, and cis-1,4-polybutadiene via molecular dynamics simulation. Soft Matter, 7 (6). 2981 - 2988 (8). ISSN 1744-683X

https://doi.org/10.1039/c0sm01086c

Soft Matter

Dynamic Article Links

Cite this: *Soft Matter*, 2011, **7**, 2981

www.rsc.org/softmatter

PAPER

Barrier properties of polyethylene terephthalate, atactic polypropylene, and *cis*-1,4-polybutadiene *via* molecular dynamics simulation

David M. Whitley and David B. Adolf*

Received 1st October 2010, Accepted 15th December 2010
DOI: 10.1039/c0sm01086c

Parallel molecular dynamics simulations have been carried out to determine the permeability of O_2, N_2, and CO_2 through polyethylene terephthalate, polypropylene and *cis*-1,4-polybutadiene. 3-dimensional (bulk) and 2-dimensional (film) periodic samples of the polymer were utilised, with the 2D film being used in two different approaches designed to probe either solubility or permeability directly. Solubility was also estimated *via* a particle insertion technique. The molecular descriptions for both polymer and gas and the analysis method were verified against experimental data. Analysis of the simulation results was *via* inter-comparison between different gases, polymers, and simulation methods. In addition, the benefits and potential shortcomings of the different simulation techniques are discussed.

1 Introduction

Understanding the passage of gas molecules through thin polymer membranes is an area of great interest, both academically and industrially. The packaging and medical industries are both examples of where understanding the mechanics of gas transport at the molecular level would be of benefit. Molecular dynamics simulations have the potential to be a valuable tool in allowing a molecular level insight to be obtained as to the processes occurring when gas molecules diffuse across a polymer boundary. This is the case for both existing barrier polymers and those potentially of interest. This work was carried out in order to investigate gas diffusion in three different polymers, using both particle insertion and molecular dynamics simulation techniques. The polymers of interest are *cis*-1,4-polybutadiene (PBD), atactic polypropylene (PP), and polyethylene terephthalate (PET). These polymers are in common use in gas sensitive applications, with used PBD in the manufacture of tyres, and PP and PET in the packaging industry.

Gas transport is often described by the solution-diffusion mechanism,[1] where gas molecules are considered to be absorbed into a polymer membrane, transported across it, and released at the other side. The solubility (S) and diffusivity (D) combine to describe the permeability (P) of a gas species in a polymer membrane as:

$$P = DS. \tag{1}$$

In order to begin to offer a complete description of the gas diffusion processes occurring inside a polymer melt, a simulation must therefore probe at least two of the above three variables. Diffusion within a polymer is traditionally described using the 'hop-and-jump' model.[2,3] This employs the idea that diffusants, in this case gas molecules, spend the majority of their time within the melt oscillating within a microscopic free volume cavity (*i.e.* 'hopping'). Occasionally, due to relaxation processes occurring within the melt, an opening between the free volume occupied by the gas molecule and a neighbouring cavity will appear. If the path between the cavities closes before the gas molecule returns to its original cavity, it has completed a 'jump'. It is with this stepwise motion that a particle diffuses within a polymer melt.

Diffusivity (D) has traditionally been probed by inserting gas molecules into a 3-dimensionally periodic (3D) sample of the polymer of interest.[4–6] The most common analysis method being to consider the mean squared displacement (MSD) of the gas molecules as a function of time (t), and to use eqn (2).[7] It is important to note that at short time the motion of the gas molecule is ballistic in nature; the gas molecule is experiencing the normal diffusive regime when $n = 1$.

$$\langle [r(t)]^2 \rangle = 6Dt^n \tag{2}$$

Solubility describes the affinity for the gas molecule to be absorbed into the melt, and is usually represented by a Henry coefficient (k_H). A system needs to contain at least two phases to be able to model sorption: a polymer membrane and a gas phase. It is not possible therefore to estimate the solubility coefficient using a single phase (bulk) polymer sample *via* molecular dynamics simulation. It is possible however to use a bulk polymer sample to estimate the solubility coefficient for a certain gas using a Widom[8] particle insertion technique. This process calculates the average excess chemical potential (μ_{ex}) which would be generated by the insertion of 1 mole of sample molecules into a polymer of interest. This is achieved by carrying out a series of randomly positioned insertions of a sample molecule

School of Physics and Astronomy, University of Leeds, Leeds, UK LS2 9JT. E-mail: d.b.adolf@leeds.ac.uk

and calculating the change in system energy (E_i) resultant from each insertion (V is the system volume, k_BT is the thermal energy, and RT is the molar thermal energy):

$$\mu_{ex} = -RT \ln\left\langle \exp\left(\frac{-E_i}{k_BT}\right)\right\rangle, \quad (3a)$$

$$\mu_{ex} = -RT \ln\left[\langle V\rangle^{-1}\left\langle V \times \exp\left(\frac{-E_i}{k_BT}\right)\right\rangle\right]. \quad (3b)$$

Eqn (3a) and (3b) are applicable in the cases where a simulation was carried out using NVT and NPT constraints respectively, with angle brackets denoting an average over both a series of random insertions and a number of different melt conformations. This excess in chemical potential can then be used to determine the Henry solubility coefficient:

$$k_{H,cc} = \exp\left(\frac{-\mu_{ex}}{RT}\right). \quad (4)$$

It is important to note at this point that the solubility can be defined in several different ways, which consequently means that there are several different Henry coefficients available for a particular system. Widom's method returns a ratio of the concentration of gas molecules within the polymer melt to the concentration of gas molecules external to the melt. This Henry coefficient is represented as $k_{H,cc}$. It is this Henry coefficient which will be calculated and quoted for all different simulation models throughout this work. The Henry coefficient usually measured experimentally is $k_{H,cp}$, which measures the dependence of the absorbed concentration of gas in the polymer melt on the partial pressure of the gas external to the melt. Conversion between the two values is achieved *via* eqn (5), where $k_{H,cp}$ has units cm^3[STP] cm^{-3} Pa^{-1}, T_{sim} is the simulation temperature in Kelvin, and P_{STP} and T_{STP} are the standard pressure and temperature (101 325 Pa and 275.15 K respectively). $k_{H,cc}$ is a unitless quantity.

$$k_{H,cc} = k_{H,cp} \times T_{sim} \times \frac{P_{STP}}{T_{STP}} \quad (5)$$

The Widom method uses infinitely fast insertions of a test particle to determine μ_{ex}, and so does not allow for the observation of the dynamic response of the polymer melt to the presence of a gas molecule,[9] hence the desire to use a molecular dynamics method to investigate permeation. Widom insertion has been commonly used for many years to determine solubility coefficients computationally[10,11] however, providing a useful benchmark against which to compare other simulation models. The Widom method can struggle for very dense systems and for large test particles, where test insertions often result in extremely high energies associated with particle overlaps. Several different methods[12–14] have been suggested for the computational assessment of the excess chemical potential in systems where Widom insertion may not be appropriate.

If a 3-dimensionally periodic sample of polymer melt is replaced by a 2-dimensionally periodic film, an external gas phase can be included. This allows for the probing of the different aspects of permeability (P, D, and S) directly in one simulation cell, in a procedure which models experimental methods. Under NPT constraints however, the absorption of gas molecules reduces the external gas pressure, which in turn leads to a reduction in the size of the external gas phase. This can lead to the external gas phase disappearing completely during long simulations. A solution to this problem was provided by Kikuchi *et al.*,[15] who filled the gas phase with 'virtual' particles. The virtual particles maintain the external pressure of the system during long NPT simulation runs, and so avoid any shrinkage of the gas phase. The particles are labelled as virtual as they have zero interaction with any gas molecules, and a purely repulsive interaction with the polymer melt. The lack of interaction with the gas molecules means that the gas molecules' behaviour is not influenced by the presence of the virtual particles. The repulsive interaction with the melt is chosen to prevent any virtual particle from entering the polymer matrix, which follows the method of Kikuchi *et al.*[15] This repulsive interaction with the melt allows the fluctuations of the NPT barostat to be imposed upon the melt, whilst maintaining a stable volume external to the melt independent of the absorption or release of gas molecules. The presence of a stable gas phase allows for a direct investigation of sorption *via* MD simulations. Two different simulation cells using the concept of virtual particles were utilised. The first approach[15] was designated "KKF1". KKF1 was initially designed solely for the determination of the solubility coefficient for a certain gas/polymer combination,[15] however, this work also utilised the KKF1 model to determine the diffusivity *via* tracking the MSD of gas molecules absorbed within the melt and application of eqn (2). Generation of a KKF1 cell involved randomly inserting varying numbers of gas molecules both above and below the 2D film. This allowed the equilibrium ratio of the absorbed gas concentration and the concentration of the gas external to the melt to be determined *via* MD simulation, giving the Henry coefficient $k_{H,cc}$ as discussed earlier. An example of the KKF1 cell is shown in Fig. 1; the melt can be seen bound by a gas phase stabilised by virtual particles.

The second approach,[16] designated "KKF2", is a variation on KKF1, implementing a concentration gradient across the melt to assess the permeability and diffusivity of a gas molecule in a polymer melt directly. This was intended to make the simulation more closely analogous to the experimental techniques used to investigate permeation.[16] The concentration gradient is generated by inserting gas molecules only into the gas phase above the melt. As gas molecules diffuse through the film and emerge on the downstream side, they are instantaneously deleted and reinserted above the film. With knowledge of the thickness of the polymer film (L), diffusivity can be estimated *via* the time lag (θ) for the first molecules to appear *via* eqn (6). If the area of the polymer gas interface (A) and difference in gas pressure between the gas phases above and below the film (Δp) are determined, permeability (P) can be estimated *via* the number (converted to a volume *via* the ideal gas law) of gas molecules that permeate through the membrane (V_{perm}) in simulation time τ *via* eqn (7).

$$D = \frac{L^2}{6\theta} \quad (6)$$

$$P = \frac{V_{perm}}{\tau} \times \frac{L}{A \cdot \Delta p} \quad (7)$$

If desired, a hybrid KKF1/KKF2 model can be used, where the permeability is still determined *via* eqn (7), but diffusivity is

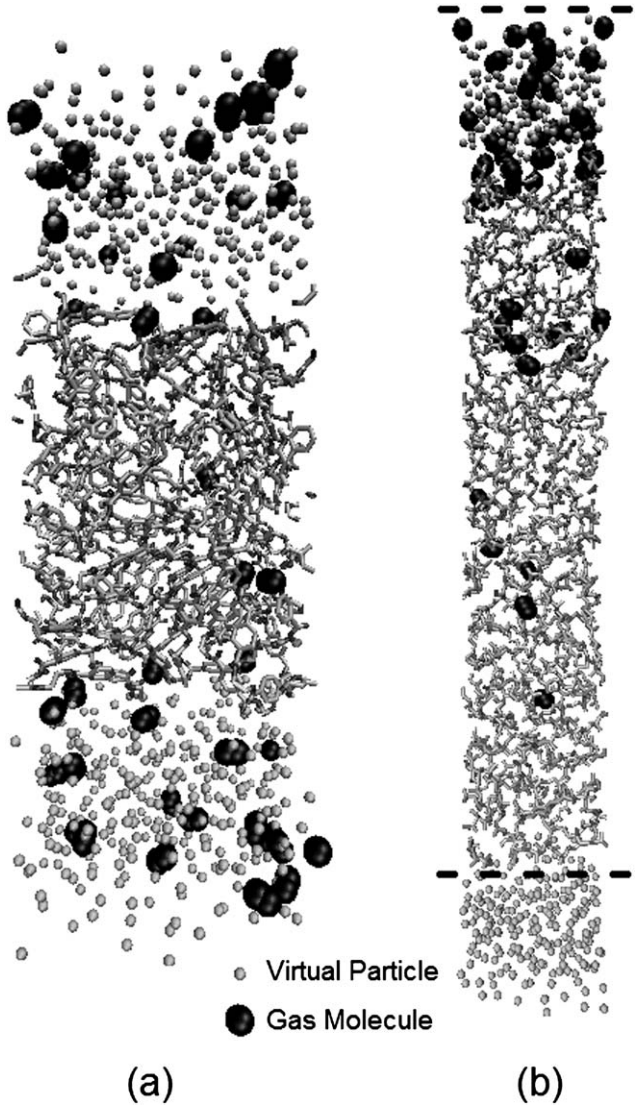

Fig. 1 Examples of the two variations on the 2D film simulation cell: (a) details KKF1, showing a PET melt absorbing diatomic gas molecules and (b) details KKF2, showing diatomic gas molecules diffusing along a concentration gradient through a PP film. Dashed lines indicate positions of repulsive walls. Note molecule sizes have been chosen for clarity only, and are not representative of any physical property. The two images are not to the same scale.

measured by tracking the mean squared displacement of all gas molecules whilst absorbed within the melt and the use of eqn (2). An example of the KKF2 cell is shown in Fig. 1, showing gas molecules diffusing through the polymer melt film along a concentration gradient.

2 Experimental method

2.1 Simulation details

Initial generation of the three polymer systems took place *via* the all *trans* chain method of Hedenqvist *et al.*,[17] with a 'skew-start'[18] being employed to ensure that chains did not overlap in 3-dimensional periodic boundary conditions. PBD was represented by 10 chains of 25 repeat units, PP by 10 chains of 50 repeat units, and PET by 4 chains of 40 repeat units. The simulated chain length was selected for each polymer to reduce computational expense, whilst ensuring that the system still accurately modelled the polymer of interest. Accuracy was ensured by verifying that the PVT and bulk diffusion behaviour at the chosen chain length were consistent with those of systems consisting of considerably longer chains, and experimental results.

Systems were generated in an extremely rarefied state, with the initial equilibration being carried out in the NVT ensemble to allow unimpeded relaxation of the polymer chains. Systems were then compressed to simulation conditions under NPT conditions, followed by a thermal equilibration in the NVT ensemble, followed by a long NPT equilibration. During the final long equilibration the centre of mass of each system was required to migrate over a distance equal to several radii of gyration of a chain in order for the system to be considered sufficiently equilibrated. The evolution of the ensemble conserved quantities, system volume, and total energy were also monitored.

PBD was described by the quantum chemistry fit data of Smith and Paul,[19] PP was described using the TraPPE-UA force field of Martin and Siepmann,[20] and PET was described by the anisotropic united atom force field of Hedenqvist *et al.*[17] Gas parameterisation was provided by Travis and Gubbins[21] (O_2, N_2) and Kikuchi *et al.*[15] (CO_2). Unlike Lennard-Jones interaction parameters, ε and σ, were computed using the standard Lorentz–Berthelot combining rules:[22,23]

$$\varepsilon_{ij} = \sqrt{\varepsilon_{ii}\varepsilon_{jj}}, \tag{8a}$$

$$\sigma_{ij} = \frac{1}{2}(\sigma_{ii} + \sigma_{jj}). \tag{8b}$$

Molecular dynamics simulations took place using the DL_POLYv2 simulation package,[24] with pressure and temperature constrained by the Nosé-Hoover method. Thermostat and barostat relaxation times were 0.5 and 0.3 ps respectively for bulk simulations, and 0.5 and 1.0 ps respectively for the two phase solubility and permeability simulation cells. Production run simulations were carried out for 40 ns, with a 2 fs timestep facilitated by the use of the SHAKE algorithm to constrain bonds. Atomic configurations were output every 1 ps.

2.2 The 3-dimensionally periodic simulation cell

Gas diffusivity within a 3-dimensionally periodic sample was assessed by inserting 10 gas molecules into the simulation cell, at positions where net non-bonding energy obeyed $-0.1\ k_BT < E_{nb} < 0.1\ k_BT$. The mean squared displacement of each molecule was monitored throughout the run, and diffusivity calculated *via* eqn (2). Diffusivity was calculated from trajectories of 0.5 ns $< t <$ 4 ns, to ensure that ballistic motion from short timescales and the poor statistics at long timescales did not distort the value obtained for the diffusivity. The selected region of a log–log MSD *vs.* t plot was required to satisfy a chi-squared goodness of fit test with respect to a slope of 1, ensuring that the above range was sampling the normal diffusive regime.

The solubility of a gas molecule in a 3-dimensionally periodic sample of the melt was assessed *via* Widom's method, as

discussed earlier. The random insertions were replaced by a grid based insertion, to ensure that the entire melt volume is sampled in a computationally efficient process. A grid spacing of 1 Å was used; this being small enough to probe all structural levels within the melt, but not so large as to make the program run time prohibitive. As all gas molecules of interest to this investigation were linear in structure, each insertion was also performed over 3 separate orientations, with the vector connecting the centres of the atoms constituting the molecule aligned in the x, y, and z direction. The net energy difference resulting from the insertion was calculated by summing the non-bonding interaction energy between the inserted molecule and each polymer atom. Electrostatic interaction energy was also included if partial charges were present in both gas and polymer. Averages were formed over 100 different trajectory frames, each well separated in time, providing the opportunity to ensure that averages were formed over many different, independent melt configurations.

2.3 The 2-dimensionally periodic simulation cells

The 2-dimensionally periodic films for the KKF1 and KKF2 simulation cells were generated using the method of Okada *et al.*[25] Films were designed to be periodic in the x/y plane, with z being perpendicular to the surface of the film. Virtual particles were formed using the parameters of Kikuchi *et al.*,[15] with the repulsive non-bonding parameters tuned to prevent any particles from entering the polymer melt. The KKF1 model had between 40 and 140 gas molecules randomly inserted into the gas phase, both above and below the 2D periodic polymer melt, creating a range of gas pressures external to the melt. Determination of the solubility and diffusivity requires knowledge of the volume of the cell occupied by the polymer melt and the external gas phase. This was achieved using the density scan method used by Kikuchi *et al.*,[15,16] with the gas phase, polymer interface, and polymer bulk identified from the density of polymer atoms scanned in the z direction. Gas molecules were therefore classified as belonging to the external gas phase, being adsorbed upon the surface of, or being absorbed within the polymer melt based upon their z-position within the simulation cell. Solubility values were estimated by counting the number of gas molecules absorbed within the melt, and considering how this absorbed concentration changed with different external gas pressure. External gas pressure is defined as the pressure of the gas molecules located in the external gas phase, as determined by the ideal gas law. Fig. 2 demonstrates the relationship between external pressure and absorbed concentration of O_2 in PBD, PP, and PET as predicted by KKF1 simulations. The good linear fit for each system indicates that the experimentally observed Henry's law is being obeyed. The solubility was determined from the gradient of this fit, whilst diffusivity was estimated by measuring the MSD of gas molecules whilst absorbed within the melt, as eqn (2). The normal diffusive regime was identified *via* a chi-squared goodness of fit test to determine where the gradient of a log–log plot was equal to unity. MSD was calculated separately for each of the simulations containing different numbers of gas molecules. As no dependence upon the penetrant concentration was noted, the final value for diffusivity was formed from average values for MSD from each simulation.

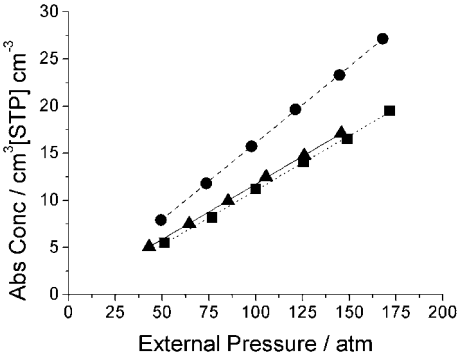

Fig. 2 Demonstration of the linear relationship between the absorbed concentration of O_2 in a PBD (circle-dashed), PP (triangle-solid), and PET (square-dotted) and the partial pressure of O_2 external to the melt in a KKF1 simulation. Symbols are simulation results; lines are least square fits from which the solubility is determined.

The KKF2 simulation cell had 50 gas molecules randomly inserted into the gas phase above the melt. To prevent the gas molecules from migrating to the bottom half of the cell *via* periodic boundary conditions, a potential wall was placed at the very top of the cell, of the form given in eqn (9), where $\varepsilon = 5000$ kcal mol^{-1}, and $n = 13$. This wall acts only upon the gas molecules.

$$U(z) = \frac{\varepsilon}{(z - z_0)^n} \tag{9}$$

The fact that gas molecules exist only in the upper gas phase causes a pressure to be exerted upon the melt which forces it downwards through the simulation cell. A potential wall of the same form and parameters as eqn (9) is included to support the bottom of the melt and so prevent this migration. This wall acts only upon the polymer atoms. When a gas molecule permeates through the melt and appears on the downstream side of the melt, it is deleted and randomly reinserted back into the upstream side of the melt. The total change in the non-bonding interaction energy resulting from the insertion must be less than $k_B T$ for the insertion to occur, preventing unphysical reinsertions. Another location for insertion is chosen if this is not the case. Fig. 3 demonstrates the permeation of O_2 molecules through PBD and PP over a 10 ns simulation. The linear fit to the data allows for the permeability to be calculated *via* eqn (7). The time lag used to determine the diffusivity *via* eqn (6) is also labelled.

3 Results

3.1 Verification of simulation models

It is important to verify that the generated configurations and molecular force fields used in an MD investigation provide an accurate description of the polymer to which they pertain. Two different verification procedures were carried out to test that this was the case. Firstly, the PVT behaviour predicted by MD simulation was compared to that observed experimentally (represented by a Tait equation). Simulations were carried out at different temperatures for each polymer, to coincide with the

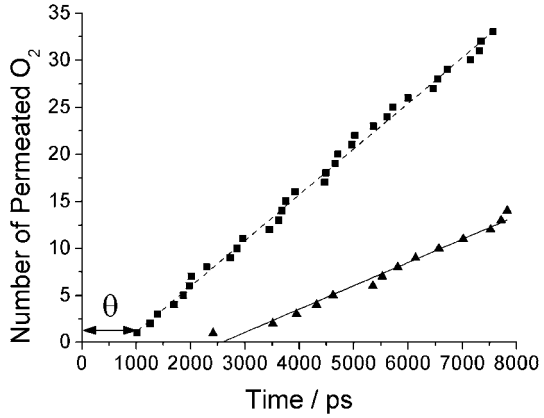

Fig. 3 Example result from the KKF2 model, showing the permeated O_2 count through PBD (square-dashed) and PP (triangle-solid), along with the linear fit from which permeability is calculated. θ, from which the diffusivity is calculated, is also labelled for PBD.

Table 1 Diffusivity of O_2, N_2, and CO_2 in PBD at 300 K, 1 atm (error bars generated from the uncertainty in linear fit)

	D ($\times 10^{-6}$ cm^2 s^{-1})		
	O_2	N_2	CO_2
This work	3.78 ± 0.01	2.12 ± 0.01	1.84 ± 0.01
Experiment[3]	1.5	1.1	1.05

Table 2 Henry solubility coefficient for O_2, N_2, and CO_2 in PBD at 300 K, 1 atm (error bars generated from the statistical deviation in repeat systems)

	$k_{H,cc}$		
	O_2	N_2	CO_2
This work	0.241 ± 0.003	0.124 ± 0.002	1.32 ± 0.06
Experiment[29]	0.105	0.050	1.08

availability of experimental data. All temperatures were well above T_g for the polymer in question.

Fig. 4 shows the PVT behaviour of the polymers of interest, and a comparison to experimental data. All polymer models show a good agreement with the experimentally observed characteristic volume at low pressures. The compressibility of both PBD and PET deviates from that seen experimentally at higher pressures (500 bar and above), a fact noted for PET by Hedenqvist *et al.*[17] in their original force field formulation. All simulations in this investigation took place at low pressure (0–250 bar), and so this deviation from experimental results at higher pressure is not an issue.

The second verification procedure was designed to test both the gas molecule parameterisation, and the routines which were to analyse the diffusivity and the solubility within the melt. Both bulk MD simulations and Widom[8] insertions were carried out at experimental conditions, to determine the diffusivity and Henry solubility coefficient of each gas molecule respectively. This was then compared to experimentally determined parameters. This verification was carried out with PBD, due to the availability of experimental D and $k_{H,cc}$ values for the gases investigated.[3,29]

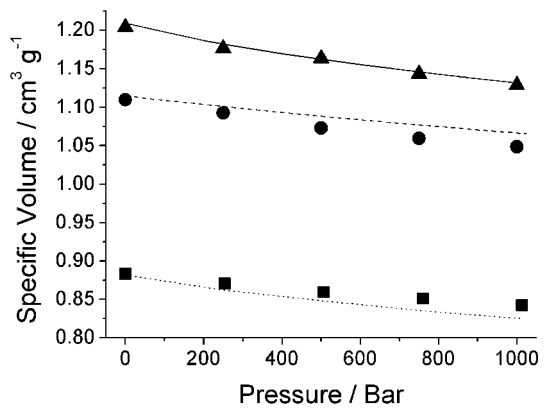

Fig. 4 Simulated (symbols) and experimentally observed (lines) PVT behaviour of PP (triangle-solid[26]), PBD (circle-dashed[27]), and PET (square-dotted[28]). Error bars are within the size of the symbol.

PBD has the lowest glass transition temperature[30] of the polymers under investigation, and so at experimental temperatures (usually approximately 300 K) will have the greatest difference from T_g. This aids the acquisition of stable MSD values for a given simulation length. Results of such verification are shown in Table 1 and Table 2, where the diffusivities and solubility coefficient of O_2, N_2, and CO_2 were determined in a PBD melt at 300 K, 1 atm.

It is reassuring to note that the simulation models correctly predict the experimentally noted trends between different gases, though there is a systematic overestimation of both diffusivity and solubility coefficient. A possible source of the systematic overestimation of the diffusivity is the limited simulated chain length leading to an overestimation of the flexibility of the polymer.[31] The source of the difference between the experimentally derived solubility coefficient and that returned from simulation is not known for certain, however Müller-Plathe *et al.*[10] noted that the trend for simulations to overestimate the solubility coefficient appears to be universal. Their proposed reasons include insufficient relaxation of the polymer melt, leading to inhomogeneous densities within the simulation cell, and small inaccuracies in the force field parameterisations.

3.2 Diffusivity

Diffusivity was estimated using all three simulation models. The estimations of diffusivity provided by the 2D film methods could be verified against bulk simulation, as bulk simulations had been shown to provide accurate values for diffusivity in the earlier verification using PBD. Table 3 presents the estimations for the diffusivity returned by the different simulation methods. All simulations were run at temperatures considerably above the T_g of the polymer in question. Simulations containing PBD and PP ran at 500 K; simulations containing PET ran at 600 K. This is due to the higher glass transition temperature of PET relative to PBD and PP. The low diffusivity of all gas species in PET prohibited the acquisition of stable diffusivity values within the given simulation timescale for KKF2. These results are not presented here.

Table 3 Estimates of diffusivity obtained from the different simulation methods (error bars generated from the statistical deviation in repeat systems)

	D ($\times 10^{-6}$ cm^2 s^{-1})		
(a)PBD—500 K	O_2	N_2	CO_2
Bulk sample	103	92.5	77.2
KKF1	126 ± 1	104 ± 6	85 ± 5
KKF2	130 ± 13	113 ± 18	110 ± 10
(b)PP—500 K	O_2	N_2	CO_2
Bulk sample	90.1	79.1	59.3
KKF1	101 ± 3	84 ± 3	74 ± 5
KKF2	115 ± 7	96 ± 8	83 ± 12
(c)PET—600 K	O_2	N_2	CO_2
Shanks and Pavel[32]	20.1	—	17.1
Bulk sample	40.8	34.8	29.5
KKF1	56 ± 2	47 ± 3	42 ± 4

It is reassuring to note that both KKF1 and KKF2 correctly predict the trends between different gas molecules within the same polymer, and between different polymer samples for the same gas molecule, although the 2D film models return values systematically higher than that of the bulk. It is also reassuring to note that the diffusivity of O_2 and CO_2 in PET returned from this work is consistent with the previous work of Shanks and Pavel,[32] subject to the tendency to overestimate reported earlier.

The statistical accuracy of the mean squared displacement within the melt reduces rapidly with increasing time when using the KKF1 model, as the majority of molecules spend only a short period of time in the melt. This is particularly the case for the high T_g polymer PET; even with simulations run at 600 K the vast majority of molecules spend less than 20 ps within the melt. Very few molecules therefore have a chance to experience the normal diffusive regime.

It was noted earlier that the accepted description of small molecule permeation through a polymer membrane is the 'hop-and jump'. One of the benefits of using molecular dynamics simulations to study gas transportation is the ability to directly visualise dynamic processes occurring within the melt. Fig. 5 demonstrates a typical z-coordinate track for a CO_2 molecule in a KKF1 simulation cell as it transits a PBD, PP, or PET film. It is interesting to note the differences between the diffusive motion in PET when compared to that in PP and PBD. In PET, the hopping periods are clearly identifiable as small magnitude oscillations, occurring between the jumps (identifiable as changes in the z position of considerably larger magnitude than the background hopping, without an immediate return to the starting point). This is not the case in PP and PBD, where the molecule transits the melt in a near continuous series of jumps. The near continual transition from jump to jump in PP and PBD is considered a result of the high temperatures at which the KKF1 simulations were carried out, when compared to T_g.

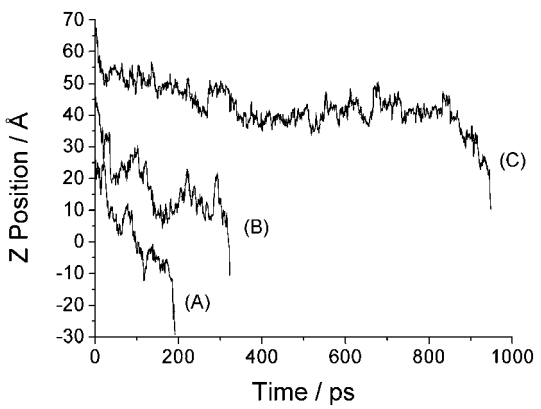

Fig. 5 Time dependence of the z position of a CO_2 molecule diffusing through 60 Å thick films of (A) PBD, (B) PP, and (C) PET. To improve clarity, the trace for PP is offset by +20 Å and PET by +40 Å.

3.3 Solubility

The KKF1 and KKF2 simulation models were designed to return either the solubility or permeability respectively, along with the diffusivity. It has been shown that the two return broadly similar diffusivities, so to facilitate comparison the permeability and diffusivity returned by KKF2 will be combined to form the solubility as in eqn (1). All solubility values are quoted as $k_{H,cc}$. As with diffusivity, acquisition of stable solubility coefficients *via* the KKF2 model in PET required prohibitively long simulation timescales, and as such values are not included here.

The solubility returned by the KKF1 model is slightly higher than that returned from the Widom method in most cases. The reason for this discrepancy is hypothesised to stem from the particle insertion technique being unable to capture dynamic details as to how the melt matrix responds to the presence of a gas molecule. The KKF2 method systematically returns considerably higher results than both 3D and KKF1 simulations. The reason for these consistently higher estimations is not fully known, however, as the uncertainties indicate, the values returned by the KKF2 model are of poorer statistical reliability than KKF1. This is due to the small numbers of gas molecules completing a transit of the film; on average between 30 and 100 gas molecules over a typical 20 ns KKF2 simulation.

Care must be taken when interpreting the results of the high temperature 2D Film simulations, as even the order of the solubility coefficients of the different gases may not be the same as at experimental conditions. For example, it can be seen in Table 4 that at a temperature of 500 K both O_2 and N_2 have a slightly higher solubility coefficient in PBD than CO_2. Table 2 shows that this is not the case at 300 K, however, with CO_2 having a markedly higher solubility coefficient than either O_2 or N_2. These observations are in agreement with the experimental findings of Cowling and Park,[33] who noted the different sign on the heat of solution of CO_2 when compared to N_2 in PBD. This means that as temperature increases, the solubility of CO_2 in PBD tends to fall, whereas the solubility of N_2 will tend to rise. It is also reported that O_2 has the same sign on its heat of solution as N_2,[29] indicating it too will become more soluble in PBD as temperature increases. This is also in agreement with the results of this work.

Table 4 Estimates of the Henry solubility coefficient obtained from the different simulation methods (error bars generated from the uncertainty in linear fit)

	$k_{H,cc}$		
(a)PBD—500 K	O_2	N_2	CO_2
Particle insertion	0.282 ± 0.001	0.245 ± 0.001	0.215 ± 0.001
KKF1	0.295 ± 0.001	0.265 ± 0.003	0.261 ± 0.001
KKF2	0.34 ± 0.05	0.31 ± 0.05	0.29 ± 0.02
(b)PP—500 K	O_2	N_2	CO_2
Particle insertion	0.209 ± 0.001	0.199 ± 0.001	0.186 ± 0.001
KKF1	0.220 ± 0.001	0.192 ± 0.002	0.184 ± 0.002
KKF2	0.27 ± 0.02	0.24 ± 0.02	0.22 ± 0.03
(c)PET—600 K	O_2	N_2	CO_2
Particle insertion	0.228 ± 0.001	0.181 ± 0.001	0.270 ± 0.001
KKF1	0.255 ± 0.004	0.222 ± 0.007	0.237 ± 0.005

3.4 Available free volume

It has been suggested that an advantage of the 2D-film methods is their ability to observe the dynamic response of the melt to the presence of gas molecules. The importance of this can be appreciated when the available free volume of a KKF1 sample of melt is considered both before and after the addition of gas molecules to the simulation cell. Available free volume was determined in a method analogous to that of Sok *et al.*[31] A test particle was grown on a series of closely spaced grid points until it touched a polymer atom, touching being defined as the separation of the atomic centres (r) satisfying:

$$r = \frac{\sigma_{\text{polymer}} + \sigma_{\text{probe}}}{2}. \quad (10)$$

This method allows the percentage of the melt accessible to a spherical probe of diameter σ_{probe} to be determined and any changes in the accessible volume when gas is present within the melt to be appreciated. The volume accessible to a probe of diameter σ_{probe} in films of PBD, PP, and PET, both with and without the presence of O_2, is shown in Fig. 6. Values are time averaged over 10 ns simulations. It can be seen that all polymer species undergo some form of change in melt conformation to accommodate gas molecules. The different responses of the various polymers to the presence of O_2 molecules is easier to visualise if the change which occurs in the availability of volume to a probe of diameter σ_{probe} is plotted, as in Fig. 7. All the polymers show an entirely positive change in available volume, indicating that the melt is swelling with the addition of gas molecules, which is in agreement with experimental observations.[34] The peak in the trace of PBD indicates that although there is an overall increase in melt volume, there is also a reduction in the frequency of smaller (<1 Å diameter) voids whilst increasing the frequency of the larger free volume expanses. The trace for PP shows a similar feature forming at very small diameter (<0.5 Å) probes, with the change in available free volume then reducing more rapidly to zero than in PBD. This indicates that the addition of O_2 molecules does not bring about the longer lengthscale changes in free volume distribution required to increase the availability of larger voids as readily in PP as in PBD at the simulation temperature of 500 K. A similar trend can be seen in PET. It can be seen that even though this polymer was simulated at 600 K, the absorption of O_2 molecules into the melt does not cause any change in the availability of volume to probes of diameter greater than 4 Å. The vast majority of the expansion of the melt is accounted for in the large increase in the available volume to probes of diameter less than 2 Å; smaller scale structural perturbations dominate. This difference in the structural response of different polymers to the presence of gas molecules absorbed within them lends support to the use of the 2D film molecular dynamics simulations as opposed to simple particle insertion for the determination of solubility.

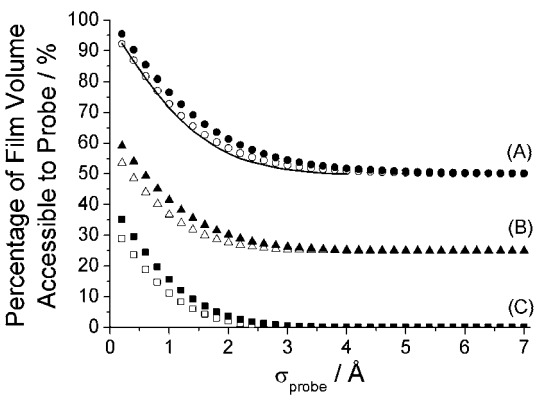

Fig. 6 Percentage of volume of a 2D film of (a) PBD (circles), (b) PP (triangles), and (c) PET (squares) accessible to a probe of varying diameter before (empty) and after (filled) the introduction of 140 O_2 molecules to the simulation cell. To improve clarity, the trace for PP is offset by +25% and PBD by +50%. Solid line is the work of Gee and Boyd[5] for PBD at 450 K.

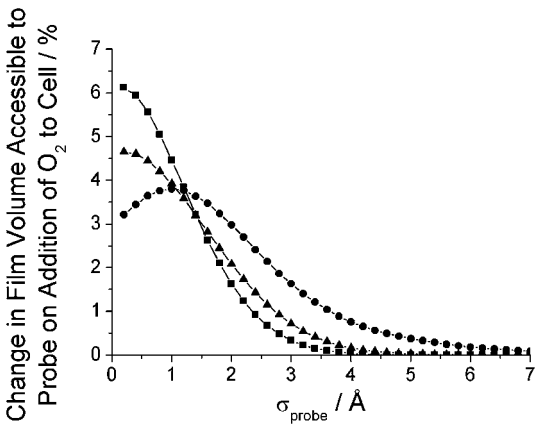

Fig. 7 The change in volume accessible to a spherical probe of varying diameter in a 2D film of PBD (circles), PP (triangles), and PET (squares) when O_2 is introduced into the simulation cell. Lines are included to aid the eye.

4 Conclusions

Permeability coefficients P, D, and S have been estimated for PBD, PP, and PET using both traditional 3D periodic (bulk) and 2D periodic (film) models. The bulk 3D polymer samples were relatively computationally economical to produce, and have been used to determine diffusivity and solubility coefficients for many

years. It has been shown that the KKF1 and KKF2 film models have the advantage that they can characterise the dynamic response of the melt to the gas molecule. The importance of this has been demonstrated by the different responses displayed by the different polymer samples to the presence of penetrant gas molecules. Encouraging agreement has been noted between these very different simulation approaches. Both the 2D film models are hampered however by the probabilistic nature of the uptake of gas molecules from the gas phase. This requires running simulations at temperatures considerably higher than those traditionally probed by experiment, meaning that verification of simulations results by comparison to experiment is difficult. Higher T_g polymers require higher simulation temperatures to retain statistical accuracy for a given simulation time, implying that the 2D film models, particularly KKF2, are generally more suited to modelling gas diffusion in lower T_g polymers.

Acknowledgements

The authors gratefully acknowledge the University of Leeds for providing a PhD scholarship for Mr D. Whitley, and for the provision of computing time on the Advanced Research Computer.

References

1 Y. Tamai, H. Tanaka and K. Nakanishi, *Macromolecules*, 1994, **27**, 4498–4508.
2 S. A. Stern, *J. Membr. Sci.*, 1994, **94**, 1–65.
3 J. Crank and G. S. Park, *Diffusion in Polymers*, Academic, New York, 1968.
4 F. Müller-Plathe, *J. Chem. Phys.*, 1991, **96**, 3200–3205.
5 R. H. Gee and R. H. Boyd, *Polymer*, 1995, **36**, 1435–1440.
6 M. Meunier, *J. Chem. Phys.*, 2005, **123**, 134906.
7 F. Müller-Plathe, *Acta Polym.*, 1994, **45**, 259–293.
8 B. Widom, *J. Chem. Phys.*, 1963, **39**, 2808–2812.
9 D. Fritz, C. R. Herbers, K. Kremer and N. F. A. van der Vegt, *Soft Matter*, 2009, **5**, 4556–4563.
10 F. Müller-Plathe, S. C. Rogers and W. F. van Gunsteren, *J. Chem. Phys.*, 1993, **98**, 9895–9904.
11 G. Tsolou, V. G. Mavrantzas, Z. A. Makrodimitri, I. G. Economou and R. Gani, *Macromolecules*, 2008, **41**, 6228–6238.
12 D. N. Theodorou, *J. Chem. Phys.*, 2006, **124**, 034109.
13 G. Boulougouris, I. G. Economou and D. N. Theodorou, *Mol. Phys.*, 1999, **96**, 905–913.
14 J. Chang, *J. Chem. Phys.*, 2009, **131**, 074103.
15 H. Kikuchi, S. Kuwajima and M. Fukuda, *J. Chem. Phys.*, 2001, **115**, 6258–6265.
16 H. Kikuchi, S. Kuwajima and M. Fukuda, *Chem. Phys. Lett.*, 2002, **358**, 466–472.
17 M. S. Hedenqvist, R. Bharadwaj and R. H. Boyd, *Macromolecules*, 1998, **31**, 1556–1564.
18 K. Refson, *Comput. Phys. Commun.*, 2000, **126**, 310–329.
19 G. D. Smith and W. Paul, *J. Phys. Chem. A*, 1998, **102**, 1200–1208.
20 M. G. Martin and J. I. Siepmann, *J. Phys. Chem. B*, 1999, **103**, 4508–4517.
21 K. P. Travis and K. E. Gubbins, *Langmuir*, 1999, **15**, 6050–6059.
22 H. A. Lorentz, *Ann. Phys. (Weinheim, Ger.)*, 1881, **248**, 127–136.
23 D. C. Berthelot, *C. R. Hebd. Seances Acad. Sci.*, 1898, **126**, 1703–1706.
24 W. Smith, C. W. Young and P. M. Rodger, *Mol. Simul.*, 2002, **28**, 385–471.
25 O. Okada, K. Oka, S. Kuwajima, S. Toyoda and K. Tanabe, *Comput. Theor. Polym. Sci.*, 2000, **10**, 371–381.
26 P. Zoller, *J. Appl. Polym. Sci.*, 1979, **23**, 1057–1061.
27 J. W. Barlow, *Polym. Eng. Sci.*, 1978, **18**, 238–245.
28 P. Zoller and P. Bolli, *J. Macromol. Sci., Part B: Phys.*, 1980, **18**, 555–568.
29 S. Pauly in *Polymer Handbook*, ed. J. Brandrup, E. H. Immergut and E. A. Grulke, Wiley, New York, 4th edn, 1999, ch. VI, pp. 543–569.
30 D. J. Plazek, and K. L. Ngai in *Physical Properties of Polymers Handbook*, ed. J. E. Mark, Springer, New York, 2nd edn, 2007, ch. 12, pp. 208–212.
31 R. M. Sok, H. J. C. Berendsen and W. F. van Gunsteren, *J. Chem. Phys.*, 1991, **96**, 4699–4704.
32 R. Shanks and D. Pavel, *Mol. Simul.*, 2002, **26**, 939–969.
33 R. Cowling and G. S. Park, *J. Membr. Sci.*, 1979, **5**, 199–207.
34 E. L. V. Lewis, R. A. Duckett, I. M. Ward, J. P. A. Fairclough and A. J. Ryan, *Polymer*, 2003, **44**, 1631–1640.

